

RESEARCH

Open Access



Cardiometabolic benefits of fenofibrate in heart failure related to obesity and diabetes

Jiwon Park^{1†}, Hangyul Song^{1†}, Shinje Moon^{2†}, Yumin Kim¹, Sungsoo Cho³, Kyungdo Han⁴, Cheol-Young Park^{5*}, Sung Woo Cho^{6*} and Chang-Myung Oh^{1*}

Abstract

Background Heart failure (HF) is a serious and common condition affecting millions of people worldwide, with obesity being a major cause of metabolic disorders such as diabetes and cardiovascular disease. This study aimed to investigate the effects of fenofibrate, a peroxisome proliferator-activated receptor alpha (PPAR α) agonist, on the obese- and diabetes-related cardiomyopathy.

Methods and results We used db/db mice and high fat diet-streptozotocin induced diabetic mice to investigate the underlying mechanisms of fenofibrate's beneficial effects on heart function. Fenofibrate reduced fibrosis, and lipid accumulation, and suppressed inflammatory and immunological responses in the heart via TNF signaling. In addition, we investigated the beneficial effects of fenofibrate on HF hospitalization. The Korean National Health Insurance database was used to identify 427,154 fenofibrate users and 427,154 non-users for comparison. During the 4.22-year follow-up, fenofibrate use significantly reduced the risk of HF hospitalization (hazard ratio, 0.907; 95% CI 0.824–0.998).

Conclusions The findings suggest that fenofibrate may be a useful therapeutic agent for obesity- and diabetes-related cardiomyopathy.

Keywords Heart failure, Fenofibrate, Diabetic cardiomyopathy

[†]Jiwon Park, Hangyul Song, and Shinje Moon have contributed equally to this work.

*Correspondence:

Cheol-Young Park
cydoctor@skku.edu

Sung Woo Cho

drswcho@hanmail.net

Chang-Myung Oh

cmoh@gist.ac.kr

¹Department of Biomedical Science and Engineering, Gwangju Institute of Science and Technology, Gwangju, Korea

²Department of Internal Medicine, Hanyang University College of Medicine, Seoul, Korea

³Division of Cardiology, Gangnam Severance Hospital, Yonsei University College of Medicine, Seoul, Korea

⁴Department of Statistics and Actuarial Science, Soongsil University, Seoul, Korea

⁵Department of Internal Medicine, Kangbuk Samsung Hospital, Sungkyunkwan University School of Medicine, Seoul, Korea

⁶Division of Cardiology, Department of Internal Medicine, Inje University Ilsan Paik Hospital, Inje University College of Medicine, Goyang, Gyeonggi-Do, Korea



© The Author(s) 2024. **Open Access** This article is licensed under a Creative Commons Attribution-NonCommercial-NoDerivatives 4.0 International License, which permits any non-commercial use, sharing, distribution and reproduction in any medium or format, as long as you give appropriate credit to the original author(s) and the source, provide a link to the Creative Commons licence, and indicate if you modified the licensed material. You do not have permission under this licence to share adapted material derived from this article or parts of it. The images or other third party material in this article are included in the article's Creative Commons licence, unless indicated otherwise in a credit line to the material. If material is not included in the article's Creative Commons licence and your intended use is not permitted by statutory regulation or exceeds the permitted use, you will need to obtain permission directly from the copyright holder. To view a copy of this licence, visit <http://creativecommons.org/licenses/by-nc-nd/4.0/>.

Background

Heart failure (HF) is a complex and common clinical syndrome characterized by impaired cardiac function resulting in inadequate blood flow and metabolic demands on the body [1]. Despite advances in HF management, the prognosis for patients with advanced HF remains poor [2]. Ten-year survival for patients with HF and left ventricular systolic dysfunction was 27.4% in the UK community-based Electrocardiographic Heart of England (ECHOES) study [3]. This highlights the need for new therapeutic options. In the US population, median survival was only 2.1 years and 5-year mortality was over 75% even in HF with preserved ejection fraction [4].

Obesity and its related metabolic disorders, especially diabetes, play a prominent role in exacerbating the prevalence of HF and the challenges associated with its management [5, 6]. The systemic inflammation and dysregulated metabolic function of the heart in individuals with obesity and diabetes is a major risk factor for the development of HF [7]. Therefore, a concerted effort to modify these metabolic abnormalities is vital for the optimal management of heart failure. Recent studies have shed light on the potential benefits of targeting metabolic pathways in the treatment of heart failure.

The Peroxisome proliferator-activated receptor (PPAR) family, which includes PPAR α , β/δ , and γ , regulates cardiac metabolism, with PPAR α serving as the major PPAR subtype in the heart [8, 9]. Numerous studies have demonstrated the beneficial effects of PPAR α activation on metabolic dysfunctions such as inflammation and insulin resistance, beyond its lipid (especially triglyceride) lowering effects [10–12]. Recent analysis from ACCORD Lipid trial revealed that fenofibrate, the PPAR α agonist, reduced the HF hospitalization and cardiovascular disease (CVD) death in type 2 diabetes patients with simvastatin [13]. In the general population, including non-diabetics, fenofibrate has been shown to significantly reduce the risk of the incidence of CVD [14]. Despite its promising therapeutic potential, the exact mechanisms by which PPAR-alpha activation mediates the observed effects of fenofibrate are not fully understood. In addition, the potential benefits of fenofibrate treatment on the prognosis of heart failure (HF) in the general population have yet to be fully elucidated in large cohort studies.

Therefore, in this study, we aimed to elucidate the underlying mechanisms of fenofibrate's beneficial effects on pathogenesis of cardiometabolic disease using db/db mice and high fat diet-streptozotocin induced diabetic mice. In addition, we investigated the effects of fenofibrate on HF hospitalization in the general population using the Korean National Health Insurance database. Our findings may provide important insights into the potential therapeutic role of PPAR α agonists in the

management of HF and related metabolic disorders, leading to the development of new therapeutic strategies.

Methods

Cell culture

H9c2 cells (rat cardiomyocytes) were purchased from the Korean Cell Line Bank (KCLB; Seoul, Korea) and were grown in Dulbecco's modified Engle's mixture (DMEM, Hyclone; Logan, USA) supplemented with 10% fetal bovine serum (FBS, Gibco™; NY, USA) and 1% penicillin/streptomycin (Welgene; Gyeongsangbuk-do, Korea). All cells were cultured in a humidified atmosphere at 37 °C with 5% CO₂.

For the experiments, H9C2 cells were seeded in a 6-well plate. Then, cells were cultured in either low glucose DMEM (1 g/L) or high glucose DMEM (4.5 g/L, Himedia; PA, USA) with fatty acid-free Bovine Serum Albumin (BSA) (Goldbio; Missouri, USA). Cells were categorized into three groups: vehicle-treated group (control), palmitate-treated group (palmitate), palmitate plus fenofibrate-treated group (palmitate+fenofibrate). Palmitate acid (Sigma-Aldrich; MA, USA) was dissolved in ethanol at a concentration of 10 mM. Fenofibrate (Sigma-Aldrich) was dissolved in DMSO.

Animals

All protocols requiring the use of animals were approved by all experiments were reviewed and approved by Institutional Animal Care and Use Committee of Gwangju Institute of Science and Technology (GIST) and studies were conducted in adherence to the NIH Guide for the Care and Use of Laboratory Animals. Euthanasia was performed by cervical dislocation while the mice were under a condition of anaesthesia. Male C57BLKS/J-Lepr (db/db) mice were purchased from the Shizuoka Institute for Laboratory Animals, Inc. (Japan SLC; Shizuoka, Japan). Mice were maintained in a 12-h light–dark cycle at ambient temperature (22±1F °C) and fed ad libitum a standard chow diet (SCD) and water. Male mice were randomly divided into two groups: db/db with corn oil (Sigma) (DB_VEH, n=4), and db/db with fenofibrate (DB_FIB, n=4). Mice were treated with either corn oil or fenofibrate between 6 and 20 weeks of age. Fenofibrate was dissolved in corn oil and injected orally at regular intervals every day at a dose of 100 mg/kg/day [15]. For type 2 diabetes mice model, male C57BL/6 J mice were purchased from the Shizuoka Institute for Laboratory Animals, Inc. (Japan SLC; Shizuoka, Japan). The 6-week-old male mice were administered an intraperitoneal injection of streptozotocin (STZ, 50 mg/kg body weight) daily for 5 days (n=8) or vehicle (n=8). The powder of streptozotocin was dissolved in 0.1 M Na-Citrate Buffer, pH 4.5. Then mice were fed with a high-fat diet ((HFD,

60 kcal% fat, D12492, Research Diets, Inc)) for 16 weeks for inducing type 2 diabetic mellitus (T2DM).

Body weight was recorded once a week, and echocardiography and glucose tolerance test (GTT) were performed one week before harvest, respectively. All experiments were carried out in accordance with the appropriate guidelines. The Institutional Animal Care and Use Committee of Gwangju Institute of Science and Technology approved all animal procedures (GIST-2021–110). Our study did not include any human data or tissue.

MTT assay for cell viability

H9c2 cells were seeded at 2×10^4 cells in each of the 96 wells and incubated overnight. Then, cells were cultured with either different drug concentrations or vehicle for 24 h, 48 h, and 72 h. The Cell proliferation kit I (Roche; IN, USA) was used for MTT (3-[4,5-dimethylthiazol-2-yl]-2,5-diphenyltetrazolium bromide) diphenyltetrazolium bromide) assay as manufacturer's protocol. Briefly, following drug treatment, the culture medium was replaced with MTT solution. After four hours of incubation, the formed formazan was dissolved in dimethyl sulfoxide (DMSO), and the absorbance at 550 and 600 nm was detected using an automated microplate reader.

Flow cytometric analysis of apoptosis

H9C2 cells were treated for 10 min at room temperature with Annexin-V-FITC (MedSystems Diagnostics; Vienna, Austria) and propidium iodide (Sigma, St. Louis, MO, USA) in binding buffer (Invitrogen™; MA, USA) [16]. The Cytoflex (Beckman counter; CA, USA) flow cytometer was used to evaluate apoptotic cells. For each sample, a total of 2×10^4 events were collected. At least three distinct experiments were used to complete the analyses in triplicate [16]. Apoptosis (Annexin V-FITC positive, PI negative) in necrotic (Annexin V-FITC positive, propidium iodide positive) cells was identified by flow cytometry [16]. Temperature, washing, and resuspension are all factors to consider.

Flow cytometry with oxidized DCFDA for ROS identification

2',7'-Dichlorofluorescein Diacetate (DCFDA, Sigma) dye was used for determining total intracellular reactive oxidative species (ROS) levels. H9C2 cells were incubated in a plate with a glass bottom for 20 min with 10 μ M DCFDA dye. Fluorescence were measured using confocal microscopy (Carl Zeiss, LSM 880 NLO) or semi-quantitatively analyzed using a flow cytometer at 488 nm and 525 nm.

Oil red O staining for H9c2 cells

The amount of intracellular lipids was measured by Oil Red O staining. To make a working solution, Oil Red O solution (Sigma-Aldrich) was dissolved in distilled water

(3:2) and diluted. H9c2 cells were fixed in 4 percent paraformaldehyde for 30 min at room temperature, washed three times in PBS, and then incubated with the Oil Red O working solution for 30 min at room temperature.

Western blot analysis

Cell lines and tissue samples was lysed in a RIPA buffer. Total protein concentrations were measured with the DC protein assay kit (Biorad; Hercules, CA). Then proteins were separated by electrophoresis and transferred to PVDF membranes. The membranes were blocked in Tris-buffered saline (TBS) containing 0.05% Tween 20 and 5% non-fat dry milk. Then membranes were incubated with specific primary antibodies (1:1,000) including Sod2 (#66,474, Proteintech; IL, USA), Fatty Acid Synthase (#3180, Cell Signaling Technology; MA, USA), PPAR α (#sc-398394, Santa Cruz Biotechnology; TX, USA) and β -Actin (#12,262, Cell Signaling Technology). After washing with TBS containing 0.05% Tween 20, membranes were incubated with HRP-linked secondary antibodies (Cell Signaling Technology) and visualized using the ECL detection kit (Merck Millipore). Signals were captured using a Luminograph II System (ATTO; Tokyo, Japan). Densitometric analysis was performed using Image J software (version 1.53).

Echocardiography

1.5–2.0% isoflurane (inhaled at 3.0 L/min) was used to anesthetize the mice, and their cardiac hypertrophy was assessed using an ACUSON NX3 Elite Ultrasound system (SIEMENS Healthineers; Munich, Germany) with a VF16-5 transducer (16.0 MHz). Echocardiographic measurements were performed as previously described [17]. The dimensions of the left ventricle (LV), the ejection fraction (LVEF), the fractional shortening (FS), the mass of the LV, and the thickness of the LV wall were all measured.

Blood analysis and glucose tolerance test

Blood samples were collected from the mice heart at the time of sacrifice. Aspartate Aminotransferase (AST), Alanine Aminotransferase (ALT), Total bilirubin (T-BIL), and lipid levels were measured at the Korea Testing & Research Institute (KTR; Jeollanam-do, South Korea), an institution authorized to perform non-clinical studies. For the glucose tolerance test, mice were fasted for around 12 h. Mice were intraperitoneally injected with 2 g/kg D-glucose in PBS. A glucometer will be used to determine the blood glucose level in tail vein blood. Blood is obtained by snipping the tail. After the glucose injection, blood glucose levels are monitored at 0, 15, 30, 60, and 120 min.

Histological examination

Cardiac tissues were harvested and fixed in 10% (w/v) neutral buffered formalin and embedded in paraffin. Sections were stained with hematoxylin–eosin (H&E). Masson's trichrome staining was performed for tissue fibrosis analysis. For lipid and fat staining, fresh collected cardiac tissues were embedded in Tissue-Tek Optical Cutting Temperature compound (Sakura; CA, USA). Then, midventricular sections were stained with oil red O and counterstained with hematoxylin.

Quantitative real-time reverse transcriptase-PCR (qRT-PCR) analysis

Total RNA was extracted with the TRIzol® reagent (Invitrogen) according to the manufacturer's protocol. Then, 2 µg of total RNA was used to generate complementary DNA with the High-Capacity cDNA Reverse Transcription kit (ThermoFisher, MA, USA). To analyze gene expression, real-time PCR was performed using the amfisure qGreen Q-PCR master mix (GenDEPOT; TX, USA). The primer sequences used in this study are provided in Supplementary Table 1.

RNA-sequencing and data analysis

RNA sequencing was performed on an Illumina HiSeq 2000 platform. Raw data was processed using the 'edgeR' package in R software (version 4.1) to generate counts per million (cpm). Then processed data were transformed to log₂ scale and standardized using quantile normalization. The adjusted log₂-cpm is then used in an integrative statistical technique to detect differentially expressed genes (DEGs). The observed T value and log₂-median-ratio between two conditions were calculated using the Student's t-test and log₂-median-ratio for each gene. To create an overall p-value, the corrected p-values were blended using Stouffer's method [18]. DEGs were chosen for each comparison based on two criteria: an overall p-value of less than 0.05 and an absolute log₂-median-ratio greater than the median of the empirical distribution's 2.5th and 97.5th percentiles.

Gene Set Enrichment Analysis (GSEA) was performed to assess the enrichment of DEGs using the R software's (version 4.1) "clusterProfiler" package [19]. Gene Ontology (GO) analysis, and Kyoto Encyclopaedia of Genes and Genomes (KEGG) analysis were performed using the DAVID program [19]. The commercial QIAGEN Ingenuity® Pathway Research (IPA®, QIAGEN Redwood City, www.qiagen.com/ingenuity) software was used to undertake an upstream regulatory analysis (URA) of DEGs detected in our analysis [20]. The p-value was calculated using Fisher's Exact Test, with 0.05 set as the significant level.

Single cell RNA-sequencing analysis

Heart tissues were dissected from the mice and dissociated into single cell suspensions using Liberase (Roche, 5,401,119,001) according to the manufacturer's protocol. The tissues were harvested in the predetermined volume (1000–1500 mm³), cut into 2–4 mm size pieces, and placed in GentleMACS C tubes with Liberase [1 mL of 1X PBS (Gibco, #10,010,023), Liberase 5 mg/ml]. Tissue dissociation was performed using the 37C_m_TDK_1 program with the GentleMACS Octo Dissociator (Miltenyi Biotec; cat. #30–093-235) and incubated in a water bath at 37 °C. After dissociation, the samples were filtered and centrifuged, the supernatant was discarded, and the sediment was resuspended in PBS.

The cell concentration of the single cell suspension was maintained at 500 cells/ul (total 1 * 10⁵ cells) and loaded onto the Chromium Next GEM Chip G Single Cell Kit (10X genomics, #1,000,120). RNA sequencing libraries were prepared using the Chromium Next GEM Single Cell 3' Kit v3.1 (10X genomics, #1,000,268). Individual libraries were diluted to 250–500 pM and sequenced on the Illumina Novaseq6000 sequencing platform using the S2 Reagent Kit (200cyc) in paired-end mode.

Gene expression matrices were generated using cellranger (v.6.1.1) with the mm10 reference genome after removal of environmental RNA using cellbender (v.0.3.0). The gene expression matrix was loaded with Seurat (v.5.0.1) and cells with less than 300 nFeature_RNA, 300 nCount_RNA and more than 80% mitochondrial ratio were excluded. Then, samples were normalized with SCTransform, 3,000 variable.features.n, and then integrated by harmony with 30 PCAs. Nearest neighbors were computed with 30 dimensions of harmony reduction. UMAP was also generated based on the 30 dimensions of harmony reductions.

Human data sources

We used the National Health Insurance Database (NHID) in Korea, established by the National Health Insurance Service in conjunction with the National Health Checkup Program [21]. This database provides longitudinal data on 97% of the South Korean population and includes de-identified sociodemographic information and insurance claims coded according to the International Classification of Diseases, 10th Revision (ICD-10). The National Health Examination Programme includes questionnaires on health status, anthropometric measurements and laboratory data. Our study protocol (2021–11-026) was approved by the Institutional Review Board of Kangbuk Samsung Hospital. As we did not access any personally identifiable information, the requirement for informed consent was waived. The study was performed according to the principles outlined in the Declaration of Helsinki.

Study design and participants

A total of 856,286 patients taking statins in Korea were prescribed fenofibrate between 2010 and 2017. Patients over the age of 40 were selected for this study, while those with a history of heart failure or missing data were excluded. Patients who developed CHF within one year of taking fenofibrate were also excluded, leaving 427,154 patients eligible for analysis. To reduce potential bias and demographic imbalance related to fenofibrate use, a fenofibrate-naive group who were also taking statins was selected from the NHID and matched to the fenofibrate-using group with 1:1 age and sex adjustment (Supplementary Fig. 4 and Table 2). The final analysis included 427,154 patients using fenofibrate and an equal number of patients not using fenofibrate. All patients were followed up until 31 December 2019.

Measurements and definitions

A standardized self-report questionnaire was used to collect information on smoking, drinking and exercise. Heavy drinking was defined as consuming 30 g or more of alcohol per day. Regular physical activity was defined as at least 30 min of moderate-intensity physical activity on five or more days per week, or at least 20 min of vigorous-intensity physical activity on three or more days per week. Those in the lowest income quintile receiving medical assistance were considered to have low household income. Obesity was defined as a body mass index (BMI) of 25 kg/m² or more. Hypertension was defined as having a blood pressure of 140/90 mmHg or higher or taking antihypertensive medication, as indicated by ICD-10 codes I10–I15. Diabetes was defined as having a fasting plasma glucose (FPG) concentration of 126 mg/dL or higher or being prescribed antidiabetic medication according to ICD-10 codes E11–E14. Chronic kidney disease (CKD) was defined as an estimated glomerular filtration rate (eGFR) of less than 60 mL/min/1.73 m², calculated using the Modification of Diet in Renal Disease study equation. Blood samples were taken after an overnight fast of at least 8 h to determine glucose, total cholesterol, triglyceride (TG), HDL cholesterol and LDL cholesterol concentrations.

Study outcomes

Incident HF was identified by hospitalization with ICD-10 codes I110, I130, I150, or I971 as the primary diagnosis. Study participants were followed from the start of the study until they were diagnosed with incident HF or until December 31, 2019, whichever came first.

Statistical analyses

Continuous variables were reported as either mean with standard deviation (SD) or median with interquartile range, while categorical variables were reported as

numbers (%). Independent samples t-test and χ^2 test were used to compare characteristics of participants at baseline. Incidence rates were reported as number of events per 1000 person-years. To examine the associations between fenofibrate and HF incidence, hazard ratios (HRs) and 95% confidence intervals (CIs) were calculated using multiple Cox regression analysis. The analysis was adjusted for potential confounding factors, including age, sex, income, smoking status, history of alcohol consumption, regular exercise, obesity, underlying diseases (such as DM, hypertension, and CKD), HDL cholesterol, TG, LDL cholesterol, and statin intensity. Subgroup analyses were performed to examine the potential effects of fenofibrate use on HF incidence based on underlying medical conditions. All data analyses were performed with SAS version 9.4 (SAS Institute, Cary, NC, USA), and a P value of less than 0.05 was considered statistically significant.

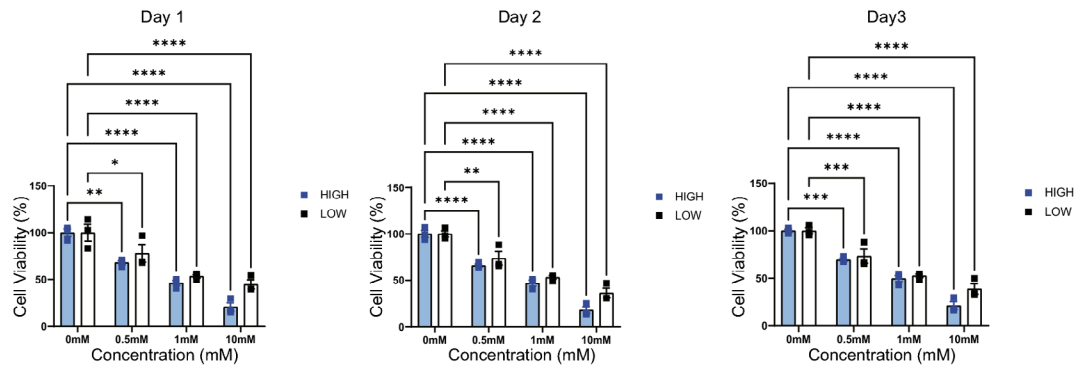
Results

Fenofibrate attenuates palmitate-induced apoptosis in H9c2 cardiomyocytes

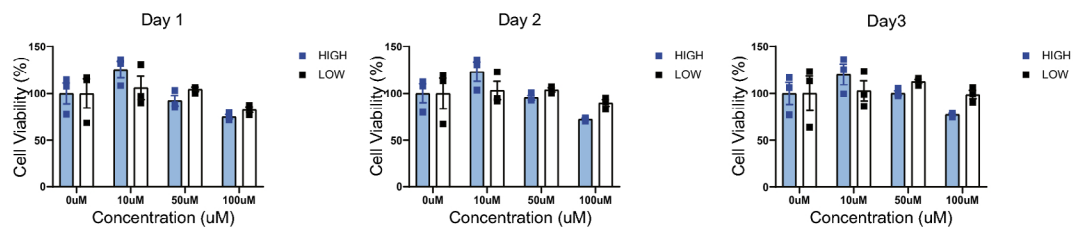
H9c2 cells were exposed to high glucose plus palmitate for 3 days to induce lipotoxicity. The MTT assay showed that high glucose plus palmitate treatment significantly reduced the viability of H9c2 cells compared to that of untreated cells (low glucose without palmitate) (Fig. 1A). Next, we investigated the protective effect of PPAR α activation in H9c2 cells against high glucose plus palmitate toxicity. Fenofibrate pretreatment prevented cell death induced by high glucose plus palmitate treatment compared to untreated cells (Fig. 1B). We performed annexin V/propidium iodide apoptosis assay to investigate the protective effect of fenofibrate against lipotoxicity-induced apoptosis. Fenofibrate significantly reduced the apoptotic cell population. Compared with the palmitate-treated group, the fenofibrate group showed reduced apoptosis (13.81% vs. 5.47%) and necrosis (9.15% vs. 4.76%), consistent with the results of the MTT assay (Fig. 1C, D). Additionally, fenofibrate treatment effectively reduced lipid accumulation in H9c2 cells (Fig. 1E, F).

Increased ROS leads to high free fatty acid concentrations in cardiomyocytes, which contributes majorly to apoptosis [22]. We performed an H₂-DCFDA assay to analyze intracellular ROS generation. Palmitate increased ROS levels in H9c2 cells, and fenofibrate treatment effectively prevented ROS generation (Fig. 2A–C and Supplementary Fig. 1A). In addition, Western blot assay showed that fenofibrate treatment increased the expressions of PPAR α and antioxidant enzymes, including Sod1 and Sod2 (Fig. 2D, E). Furthermore, fenofibrate treatment effectively reversed the changes in GLUT4 and CD36 expression induced by palmitate treatment (Supplementary Fig. 1B).

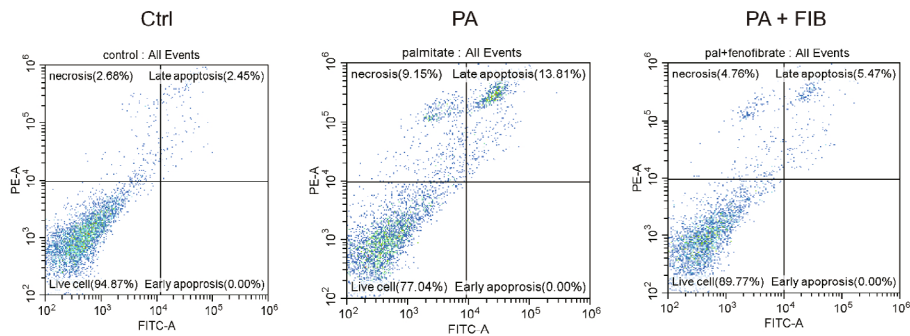
(A) Palmitate



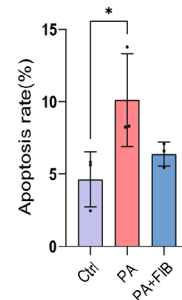
(B) Fenofibrate



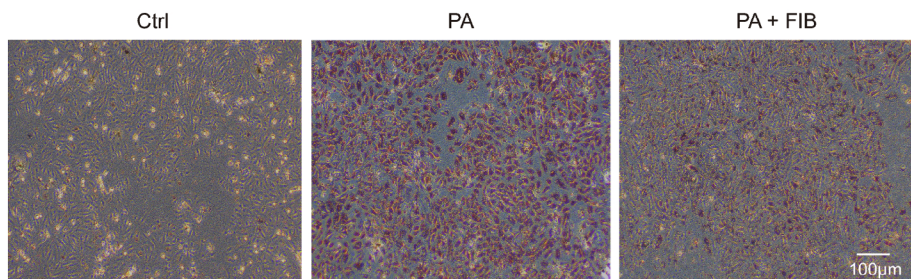
(C)



(D)



(E)



(F)

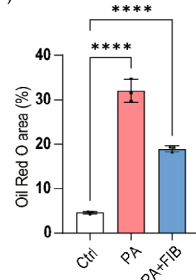


Fig. 1 **A** Effect of palmitate and fenofibrate on H9C2 cell viability Cell viability was measured using MTT Assay, and concentrations were 0.5 mM, 1 mM, and 10 mM, respectively. Measurements were carried out for 3 days (n = 3 per group). **B** Fenofibrate was treated with 10 µM, 50 µM, and 100 µM based on the Palmitate 0.5 mM set in (A) for 3 days (n = 3 per group). **A, B** Then normalized to controls. **C, D** Apoptosis was measured using flow cytometry. Each group had three samples, and all experiments were repeated three times. All controls were treated with 0.05% DMSO. *P < 0.05. **E** H9C2 cells were stained with Oil Red O dye. Control (without treatment). Stimulation with PA (500 µM). Fenofibrate was treated at 10 µM with PA (500 µM), scale bar: 100 µm. **F** Using Image J (n = 3 per group), the area stained with oil red o was measured. Data correspond to mean ± SEM per group to measure the percentage of lipid accumulation. ****P 0.0001, ***P < 0.001, **P < 0.01, *P < 0.05. Significant differences were determined by using a two-way ANOVA

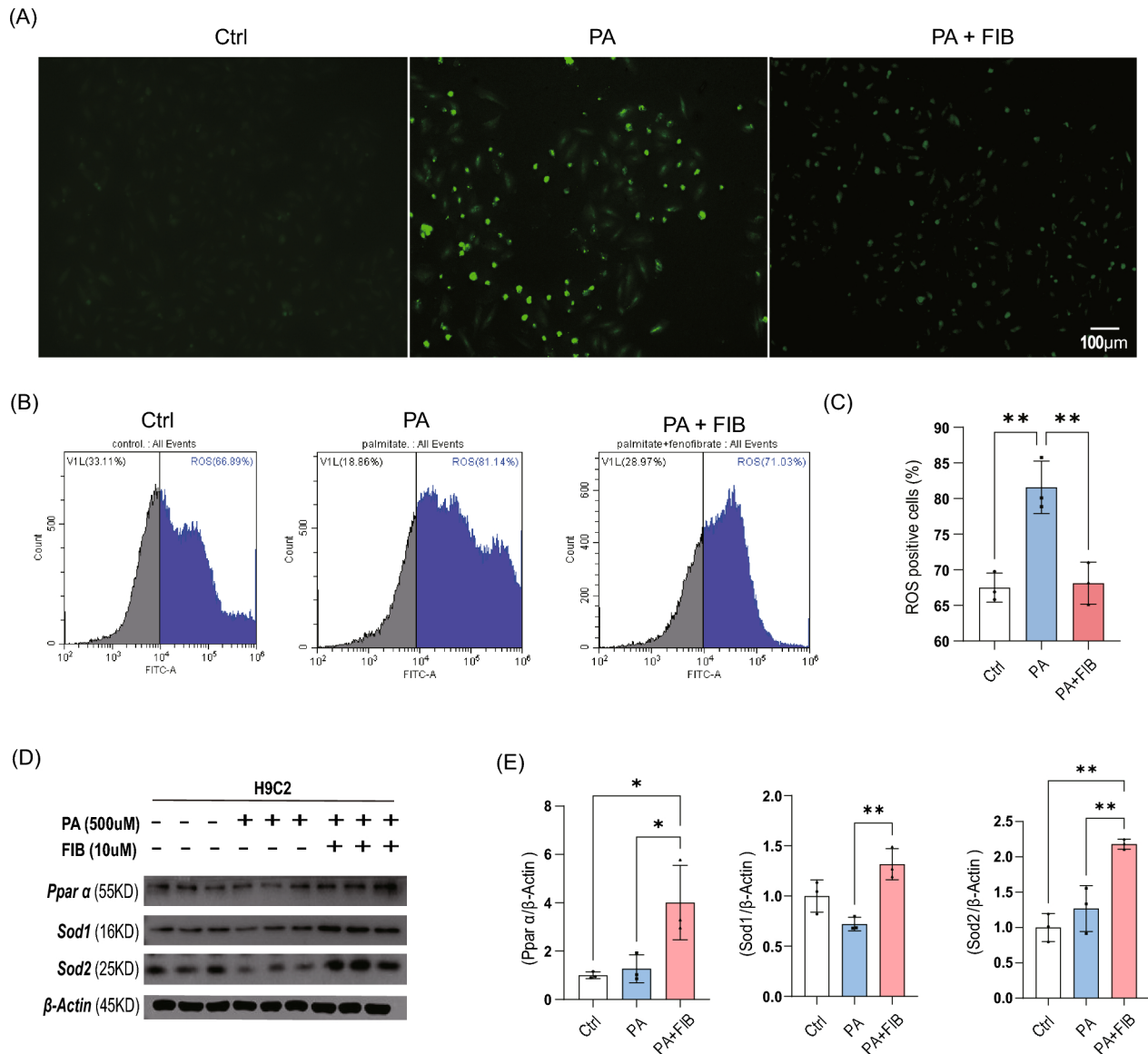


Fig. 2 **A** Staining H9C2 with H2-DCFDA, scale bar: 100 μ m. **B** Multiple gating of cells arrested with H9C2 together with H2-DCFDA by flow cytometry (n=3 per group). **C** ROS value statistical values expressed as percentage (value of area where ROS level shifted to the right) (n=3 per group). **D** Western blot was performed to determine the expression of proteins. Ppar α , Sod1, and Sod2 proteins were detected by co-addition of palmitate and fenofibrate to H9C2 (n=3 per group). **E** Quantitative values were adjusted to β -actin. Values quantified as relative expression values of Ppar α , Sod1, and Sod2. Data are expressed as mean \pm SEM. **P < 0.01, *P < 0.05 compared to control group. Two-way ANOVA was used to determine significant differences (n=3 per group). Significant differences were determined by using a two-way ANOVA

Fenofibrate enhanced cardiac function in db/db mice

We assessed the protective effects of PPAR α activation in vivo using diabetic db/db mice, which is a well-established animal model for obesity-related cardiomyopathy [23]. We administered either corn oil (vehicle, DB_VEH group) or fenofibrate (DB_FIB group) to db/db mice for 8 weeks. The DB_FIB group showed reduced weight gain and improved glucose tolerance compared to the DB_VEH group during this period (Supplementary Fig. 2A, B). Echocardiography was performed to determine whether fenofibrate prevented cardiomyopathy

in db/db mice (Fig. 3A). Fenofibrate treatment significantly reduced LV mass, enhanced LVEF, and reduced FS (Fig. 3B). Moreover, histological analysis showed that fenofibrate treatment was effective in reducing both cardiac fibrosis (Fig. 3C and Supplementary Fig. 2D) and lipid accumulation (Fig. 3D and Supplementary Fig. 2E) compared with the control group.

Fenofibrate is widely administered to patients with dyslipidemia and acts as a lipid-modifying agent by activating PPAR α signaling [24]. Fenofibrate significantly reduced total cholesterol and triglycerides (TG) and

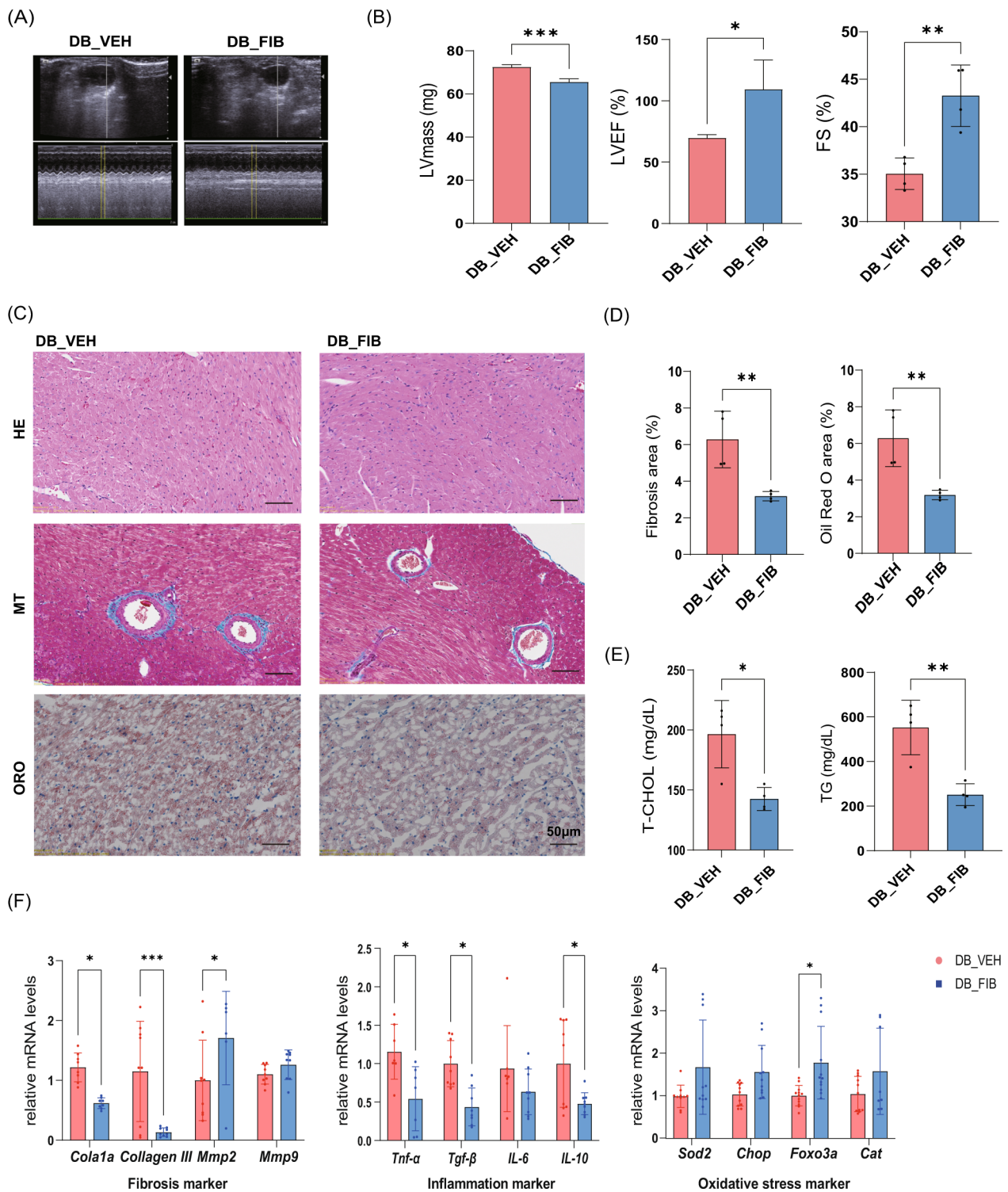


Fig. 3 A db/db vehicle and fenofibrate mice M-mode and 2D echocardiography Mice were anesthetized and cardiac function was assessed using echocardiography (n=4 per group). **B** Numerical LV mass, LVEF, FS for cardiac function using echocardiography. **C** Each group underwent Hematoxylin and Eosin (H&E) staining, Masson's trichrome and oil red o staining of sections cut relative to the atrium (n=4 per group). **D** Percentage of fibrosis (collagen content) in healthy heart muscle as measured by Masson's trichrome in muscle sections, scale bar: 100 μ m. Data correspond to mean \pm SEM per group (n=4 per group). **E** Serum T-CHO, TG were measured (n=4 per group). **F** The mRNA expression of heart failure indicators, inflammatory markers, and oxidative stress-related genes. Results were expressed as mean SD where β -actin was used as a loading control. Data were normalized using beta-actin expression (n=4 per group) via t-test. ***P < 0.001, **P < 0.01, *P < 0.05 compared with control. Significant differences were determined by using a two-way ANOVA

increased HDL cholesterol in the blood of db/db mice (Fig. 3E and Supplementary Fig. 2C). Fenofibrate also reduced serum levels of the liver damage markers alanine aminotransferase (ALT) and aspartate aminotransferase (AST) in db/db mice (Supplementary Fig. 2C). Fibrosis- and inflammation-related mRNA expression was significantly reduced in the hearts of the DB_FIB group compared to that in the DB_VEH group in the qPCR analysis (Fig. 3F). In contrast, antioxidant genes, including *Foxo3a* (Forkhead Box O3) [25], were upregulated in the DB_FIB group compared with the DB_VEH group (Fig. 3F).

Transcriptome signatures of PPAR α activation in mice hearts

We performed RNA-seq and analyzed cardiac transcriptomic signatures of DB_VEH and DB_FIB to further elucidate the mechanisms of the protective effect of PPAR α activation on DCM. The volcano plot (Fig. 4A) shows the results of the DEG analysis of the two groups. The top three upregulated genes were Zinc finger protein 69 (*Zfp69*), Glucokinase (*Gck*), and Cystathionine-gamma-ligase (*Cth*). The top three downregulated genes were Fos proto-oncogene (*Fos*), Nuclear receptor subfamily 4 group A member 1 (*Nr4a1*), and Apolipoprotein L domain containing 1 (*Apold1*). Next, we conducted GO and KEGG pathway analysis to identify the critical pathways in the heart tissues of the DB_FIB group compared with that of the DB_VEH group. PPAR α activation led to a positive enrichment of mitochondrial-related pathways, including “NADH dehydrogenase complex assembly,” “mitochondrial gene expression,” and “oxidative phosphorylation.” PPAR α activation also led to negative enrichment of inflammation- and fibrosis-related pathways, including “cytokine production” and “TNF signaling” pathways (Fig. 4B and C).

We performed upstream regulator analyses (URA) using QIAGEN's Ingenuity[®] Pathway Analysis (IPA) tool to identify potential upstream regulators, including transcription factors, cytokines, receptors, kinases, genes, or chemicals [20]. The top 17 inhibited and top nine activated upstream regulators are listed in Table 1. Prostaglandin E receptor 2 (*Ptger2*) was the most powerful predicted inhibitor (Z-score = -3.293), and growth factor-independent 1 transcriptional repressor (*Gfi1*) was the most powerful predicted activator (Z-score = 2.918) among the 26 upstream regulators. Tumor necrosis factor (TNF) was a significant predicted inhibitor (Z-score = -2.146), and interferon beta 1 (*Ifnb1*) was a significant predicted activator (Z-score = 2.274) among the cytokines. Next, we investigated interactions between PPAR α activation responsive genes. Genes or gene products, including enzymes, cytokines, receptors, and other proteins, are shown as nodes, and molecular/

biological interactions are shown as lines (Fig. 4D). The color of the node represents the degree of upregulation (red) or downregulation (blue). Grey nodes are non-DEGs. Figure 4D shows the core networks identified using IPA. These networks were categorized into three groups (Supplementary Fig. 3). These groups contained immunity-related genes (Supplementary Table 2). The main molecules in this network were TNF- and C-C motif chemokine receptor-like 2 (*Ccr12*).

Baseline characteristic of the participants

The participants' baseline characteristics are listed in Table 2. The mean age of participants was 57.9 years, and over half (54.2%) were men. Nearly half (49.8%) of the participants were obese, 24.4% had diabetes, 54.8% had hypertension, and 6.9% had CKD. During the 4.22-year follow-up, heart failure occurred in 2,066 participants (0.24%). Individuals in the fenofibrate group were more likely to be current smokers and heavy drinkers, less likely to exercise regularly, and had lower household incomes than those in the fenofibrate-naïve group. In addition, the fenofibrate group had a higher prevalence of obesity, diabetes, hypertension, and CKD compared to the fenofibrate-naïve group. Waist circumference, blood pressure, and fasting plasma glucose (FPG) levels were higher in the fenofibrate group compared to the fenofibrate-naïve group, whereas HDL and LDL cholesterol levels were lower. The fenofibrate group had a mean concentration of 215.9 mg/dL, which was higher than the 125.6 mg/dL of the fenofibrate-naïve group.

Clinical benefits of fenofibrate in the prevention of HF hospitalizations

The risk of HF was significantly lower in the fenofibrate group than in the fenofibrate-naïve group (Hazard's ratio [HR], 0.907; 95% confidence interval [CI], 0.824–0.998) after adjusting for confounding factors, including age, sex, smoking status, heavy alcohol consumption, regular physical activity, low income, the presence of obesity, hypertension, DM, and CVD, and TG, HDL cholesterol, and LDL cholesterol levels (Fig. 4E). Further analyses based on various medical conditions showed that the fenofibrate group had a reduced risk of HF in the following subgroups: obesity (HR, 0.866; 95% CI 0.762–0.985), hypertension (HR, 0.89; 95% CI, 0.801–0.988), and CKD (HR, 0.769; 95% CI, 0.644–0.919) subgroups. Specifically, the fenofibrate group had a significantly lower risk of heart failure than the fenofibrate-naïve group in the subgroups of individuals with LDL levels < 130 mg/dL (HR, 0.819; 95% CI, 0.729–0.92) and those with TG levels > 200 mg/dL (HR, 0.847; 95% CI 0.718–0.998) (Table 3). These findings suggest that fenofibrate may have protective effects against HF in individuals with certain medical

Table 1 Upstream regulator analysis with IPA

Upstream regulator	Molecule type	Predicted activation state	Activation Z-score	P-value of overlap	Target molecules in dataset
PTGER2	g-protein coupled receptor	Inhibited	- 3.293	4.57E-05	CXCR4,HDC,IL1B,KIF11,MKI67,MMP9,PRC1,PTGS2,STIL,TNF,TPX2
GLI3	Transcription regulator	Inhibited	- 2.828	2.48E-06	DUSP1,DUSP2,DUSP5,EGR1,FOSB,JUNB,KLF2,NFKBIZ
BHLHE40	Transcription regulator	Inhibited	- 2.649	1.42E-04	AHR,ATF3,C3AR1,CCN4,CCR1,CCRL2,CD14,CD74,EREG,GBP6,HAS1,IFI16,IL2RB, JCHAIN,NLRP3,PDE4B,PTGS2,RGS1,RGS16,SIHA2,SREBF1,TENT5A,TNF,UPP1
MYD88	Other	Inhibited	- 2.63	4.37E-07	CCRL2,CD40,CEBPD,CXCL13,CXCL2,DUSP1,EGR1,HDC,IFIT1B,IL1B,MKI67,MMP9, NFKBIA,NFKBIZ,NLRP3,PDE4B,PILRA,PTGS2,S100A8,TNF
MARK2	Kinase	Inhibited	- 2.449	1.70E-04	CXCL2,HDC,ligp1,NFKBIZ,PTGS2,TNF
NFAT5	Transcription regulator	Inhibited	- 2.383	4.23E-02	CD40,DUSP6,IFIT1B,IL1B,Mx1
TAZ	Enzyme	Inhibited	- 2.335	1.21E-06	CXCL2,IL1B,S100A8,S100A9,TNF
PDK1	Kinase	Inhibited	- 2.236	1.36E-04	IL1B,MLXIPL,NQO1,SCD,SREBF1
SERPINE1	Other	Inhibited	- 2.236	1.94E-05	ATP6V0D2,CCRL2,CD14,DUSP2,EDN1,HDC,IL1B,MYCN,PPP1R15A,PTGS2,TNF
SOCS6	Other	Inhibited	- 2.236	8.20E-04	CDKN1A,CXCL2,CXCR4,IL1B,JUN,PTGS2,TFRC
TRAF3IP2	Enzyme	Inhibited	- 2.224	2.02E-05	CD40,CEBPD,CXCL13,CXCL2,EREG,IL1B,IRF4,MMP9,NFKBIA,NFKBIZ,PTGS2,TIMP1, TNF,TNFRSF18
FOXO1	Transcription regulator	Inhibited	- 2.202	1.60E-05	CD14,EGR1,GJA1,IL1B,LTf,PTGS2,TNF
AGER	Transcription regulator	Inhibited	- 2.2	5.29E-05	CEBPD,CXCL2,HDC,ligp1,NFKBIA,Retnla,TNF,ZFP36
MAPKAPK2	Kinase	Inhibited	- 2.176	1.36E-04	IL1B,MMP9,S100A8,S100A9,TNF
KITLG	Growth factor	Inhibited	- 2.158	1.13E-01	ATP6V0D2,GFPT2,IL7R,KLF2,KLF4,RAG1
TNF	Cytokine	Inhibited	- 2.146	3.16E-02	CDH3,CXCL2,IL1B,MMP9,TNF
HIF1A	Transcription regulator	Inhibited	- 2.023	3.55E-04	CEBPD,CXCL2,IL1B,PTGS2,TNF
CISH	Other	Activated	2.111	7.72E-04	CES1,DBP,HLA-DQB1,PLAU,SPON2
ARNTL	Transcription regulator	Activated	2.159	6.21E-02	ADIPOQ,CARD11,CD3G,ITK,LCK
SIGIRR	Trans-membrane receptor	Activated	2.216	2.38E-02	CCRL2,CD40,CXCL2,CXCR4,CYTIP,HLA-A,IGHM,IGKC,IL1B,IRF4,TIMP1,TNF
IFNAR1	Trans-membrane receptor	Activated	2.219ra>	5.21E-09	CD74,HLA-DMB,HLA-DQB1,HLA-DRB5,Hspa1b,IFI16,IFIT1B,IFIT3,ligp1,IRGM,Mx 1,Mx2
IFNB1	Cytokine	Activated	2.274	1.70E-04	CXCL2,HDC,ligp1,NFKBIZ,PTGS2,TNF
BCL3	Transcription regulator	Activated	2.401	4.37E-07	CCRL2,CD40,CEBPD,CXCL13,CXCL2,DUSP1,EGR1,HDC,IFIT1B,IL1B,MKI67,MMP9, NFKBIA,NFKBIZ,NLRP3,PDE4B,PILRA,PTGS2,S100A8,TNF
NR1H	Ligand-dependent nuclear receptor	Activated	2.596	1.42E-04	AHR,ATF3,C3AR1,CCN4,CCR1,CCRL2,CD14,CD74,EREG,GBP6,HAS1,IFI16,IL2RB, JCHAIN,NLRP3,PDE4B,PTGS2,RGS1,RGS16,SIHA2,SREBF1,TENT5A,TNF,UPP1
PRDM1	Transcription regulator	Activated	2.63	2.48E-06	DUSP1,DUSP2,DUSP5,EGR1,FOSB,JUNB,KLF2,NFKBIZ
GFI1	Transcription regulator	Activated	2.918	4.57E-05	CXCR4,HDC,IL1B,KIF11,MKI67,MMP9,PRC1,PTGS2,STIL,TNF,TPX2

Table 2 Baseline characteristics of the study population according to the use of fenofibrate

	Total	Fenofibrate		p-value
		Non-user	User	
N	854,308	427,154	427,154	
Males, %	463,260 (54.23)	231,630 (54.23)	231,630 (54.23)	
Age, years	57.93 ± 9.59	57.93 ± 9.59	57.93 ± 9.59	
40–64	640,504 (74.97)	320,252 (74.97)	320,252 (74.97)	
≥ 65	213,804 (25.03)	106,902 (25.03)	106,902 (25.03)	
Low income	177,493 (20.78)	84,769 (19.85)	92,724 (21.71)	< 0.0001
Current smoker	189,851 (22.22)	85,375 (19.99)	104,476 (24.46)	< 0.0001
Heavy alcohol consumption	366,748 (42.93)	175,985 (41.2)	190,763 (44.66)	< 0.0001
Regular physical activity	182,690 (21.38)	96,369 (22.56)	86,321 (20.21)	< 0.0001
Obesity	425,523 (49.81)	192,162 (44.99)	233,361 (54.63)	< 0.0001
Diabetes	233,735 (27.36)	97,284 (22.77)	136,451 (31.94)	< 0.0001
Hypertension	468,095 (54.79)	219,507 (51.39)	248,588 (58.2)	< 0.0001
Chronic kidney disease	58,945 (6.9)	27,978 (6.55)	30,967 (7.25)	< 0.0001
Statin intensity				< 0.0001
Low	79,182 (9.27)	15,584 (3.65)	63,598 (14.89)	
Middle	753,369 (88.18)	400,915 (93.86)	352,454 (82.51)	
High	21,757 (2.55)	10,655 (2.49)	11,102 (2.6)	
BMI	25.15 ± 3.14	24.79 ± 3.15	25.51 ± 3.1	< 0.0001
Waist circumference	84.72 ± 8.5	83.68 ± 8.62	85.77 ± 8.25	< 0.0001
Fasting plasma glucose, mg/dL	111.32 ± 36.27	107.53 ± 32.49	115.1 ± 39.32	< 0.0001
Systolic blood pressure, mm Hg	127.28 ± 15.04	126.21 ± 14.92	128.34 ± 15.08	< 0.0001
Diastolic blood pressure, mm Hg	78.81 ± 10.07	78.11 ± 10	79.5 ± 10.09	< 0.0001
Total cholesterol, mg/dL	211.2 ± 47.35	208.62 ± 46.79	213.78 ± 47.78	< 0.0001
HDL cholesterol, mg/dL	52.09 ± 16.27	54.71 ± 16.59	49.48 ± 15.51	< 0.0001
LDL cholesterol, mg/dL	121.57 ± 44.79	125.65 ± 43.49	117.49 ± 45.7	< 0.0001
Triglyceride, mg/dL	197.75 ± 130.86	143.8 ± 83.23	251.7 ± 146.62	< 0.0001
Heart failure	2066 (0.24)	996 (0.23)	1070 (0.25)	0.1031
F/U Duration				
Mean ± SD	4.22 ± 2.15	4.22 ± 2.15	4.23 ± 2.15	0.3806
Median (Q1-Q3)	4.06 (2.35–5.84)	4.05 (2.35–5.84)	4.06 (2.35–5.84)	0.5177

Data are presented as mean ± standard deviation

HDL high-density lipoprotein, LDL low-density lipoprotein, eGFR estimated glomerular filtration rate

Table 3 Hazard ratios of heart failure related hospitalization based on the fenofibrate use status

	Hazard ratio	Lower limit	Upper limit	p-Value	Hazard ratio and 95% CI
Total	0.907	0.824	0.998	0.046	
Obesity	0.866	0.762	0.985	0.028	
DM	0.918	0.801	1.053	0.221	
Hypertension	0.890	0.801	0.988	0.029	
CKD	0.769	0.644	0.919	0.004	
LDL-C < 130	0.819	0.729	0.920	0.001	
LDL-C ≥ 130	1.068	0.918	1.243	0.395	
Triglyceride < 200	0.916	0.814	1.030	0.143	
Triglyceride ≥ 200	0.847	0.718	0.999	0.048	

conditions, including dyslipidemia and high triglyceride levels.

Fenofibrate alleviates cardiac dysfunction in high fat diet/streptozotocin-induced diabetic mice

Next, we assessed the protective effects of fenofibrate in HFD/STZ-induced diabetic (T2D) mice model, which is

a widely used animal model for DCM [26]. We divided C57BL/6J mice into three groups: control group (mice with standard chow diet feeding), HFD+STZ group (T2D mice), Fenofibrate group (T2D mice with fenofibrate). After 16 weeks of fenofibrate treatment, the Fenofibrate group showed reduced weight gain and improved glucose tolerance compared to the HFD+STZ group (Supplementary

Fig. 5A, B). Fenofibrate treatment significantly enhanced LVEF, reduced FS, and improved diastolic dysfunction (Fig. 5A, B). Moreover, histological analysis showed that fenofibrate treatment was effective in reducing both cardiac fibrosis and lipid accumulation compared with the control group (Fig. 5C). Western blot analysis revealed that Sod2 and Sirt2 protein levels were decreased in HFD+STZ compared to the control group. This reduction was reversed by fenofibrate (Fig. 5D).

To understand the molecular mechanism of the beneficial effects of fenofibrate in both non-cardiomyocytes as well as cardiomyocytes in the diabetic heart, we performed single-cell RNA sequencing and characterized gene expression profiles of cardiac cells from HFD+STZ group (n=2) and Fenof group (n=2). After quality control, normalization, and manual annotation of the cell clusters using known signature genes, we identified 12 cell types (Fig. 5E and Supplementary Fig. 5C). Based on DEGs in each cardiac cell identified by Seurat's FindAllMarkers' function (using the standard Wilcoxon rank sum test) [27], we calculated the module score related to 'cardiac muscle contraction'. HFD reduced gene expressions related to myocardial contraction, and fenofibrate treatment significantly reversed this reduction in cardiac cells (Fig. 5F).

Endothelial dysfunction is the key pathogenic event in the pathogenesis of DCM [28, 29]. The apolipoprotein L domain containing 1 (*Apold1*) is a secreted lipoprotein [30] and has shown various role including angiogenesis under hypoxic condition [31], inflammatory response [32], and stress response [33]. In the T2D group, the gene expression of *Apold1* in cardiac endothelial cells was increased compared to the control group and reversed by fenofibrate treatment (Fig. 5G). GSEA also revealed that genes related to 'TNF signaling pathway' showed negative enriched score in endothelial cells (Fig. 5H). The Low-density lipoprotein receptor-related protein 1 (*Lrp1*) has shown negative associations with inflammatory response, vascular disease, and fibrosis [34, 35]. In the mouse heart, the *Lrp1* gene was highly expressed in fibroblasts (Fig. 4B in the Supplementary Fig. 5D). In fibroblasts, *Lrp1* genes were decreased in the T2D group compared to the control group and reversed by fenofibrate treatment (Fig. 5I).

Discussion

Obesity-related metabolic dysfunctions such as hyperglycemia, insulin resistance and high free fatty acid flux drives the lipid overstorage in cardiac myocytes, known as cardiac steatosis, which causes lipotoxicity, oxidative stress, inflammation and subsequent heart failure [36–38]. In this study, we hypothesized that fenofibrate treatment may enhance the cardiac function of mice with obesity-related cardiomyopathy. Because PPAR α activation by fenofibrate has beneficial consequences on

glucose homeostasis, insulin resistance, inflammation as well as hyperlipidemia in other peripheral tissues such as pancreatic beta cell, liver, and adipose tissue [39–42].

Our study shows that fenofibrate improved the structure and function of obesity-related cardiomyopathy and DCM. In vitro experiments using H9c2 cells shows that fenofibrate reduced glucolipotoxicity induced ROS and decreased apoptosis of cardiomyocytes. In addition, fenofibrate treatment improved cardiac function, reduced intracellular lipid accumulation and fibrosis in heart tissues of *db/db* mice and T2D C57BL/6 J mice. Fenofibrate treatment increased the expression of SIRT3 and SOD2 in the heart (Figs. 2 and 5). The SIRT3-SOD2 pathway plays a protective role against metabolic stress in cardiac tissue [43, 44]. Therefore, activation of SIRT3 by PPAR α may be a key mechanism underlying the beneficial effects of fenofibrate on the heart. In line with previous studies [39, 40], fenofibrate-treated mice showed improved glucose homeostasis, reduced hepatocellular injury markers and triglyceride, and increased HDL cholesterol in blood. These findings suggest that PPAR α activation could be a promising option for the treatment of HF.

For further investigation of molecular mechanisms of PPAR α action on the obese heart, we analyzed transcriptome of fenofibrate treated heart tissue. We discovered potential therapeutic targets and underlying mechanisms of PPAR α action. *Nr4a1* and *Nr4a2* genes are most highly downregulated DEGs in the DB_FIB group compared to DB_VEH group, which encode *Nr4a1* and *Nr4a2*. These nuclear receptors are subfamily of orphan nuclear receptors and regulate glucose and lipid metabolism in the liver, skeletal muscle and adipose tissue [45]. *Nr4a1* knock out mice fed high fat diet (HFD) showed increased hepatic steatosis, intramuscular TG accumulation, and increased fat mass [45]. In the heart, *Nr4a1* gene expressions are increased in the heart of HFD-fed mice, and regulate glucose metabolism and heart functions [46]. *Nr4a* members participates in renin-angiotensin system and play a key role in cardiac remodeling [47]. These findings indicate that inhibiting *Nr4a* signaling with fenofibrate may be a feasible therapeutic strategy for HF.

Core-network analysis also revealed possible mechanisms of PPAR α action on the obese and diabetic heart. All three clustered groups composing core-networks are related to immune cell regulations. Furthermore, most significant downregulated genes in the networks are proinflammatory molecules such as TNE, interleukin 1 beta, C-X-C motif ligand 13. Previous studies also reported that PPAR α regulates innate immunity [48], and suppresses inflammatory cytokine levels [49]. These findings suggest that immune system modulation is essential to the protective role of PPAR α activation in obese and diabetic hearts. Single cell RNA sequencing analysis revealed that PPAR α action on the EC cells and

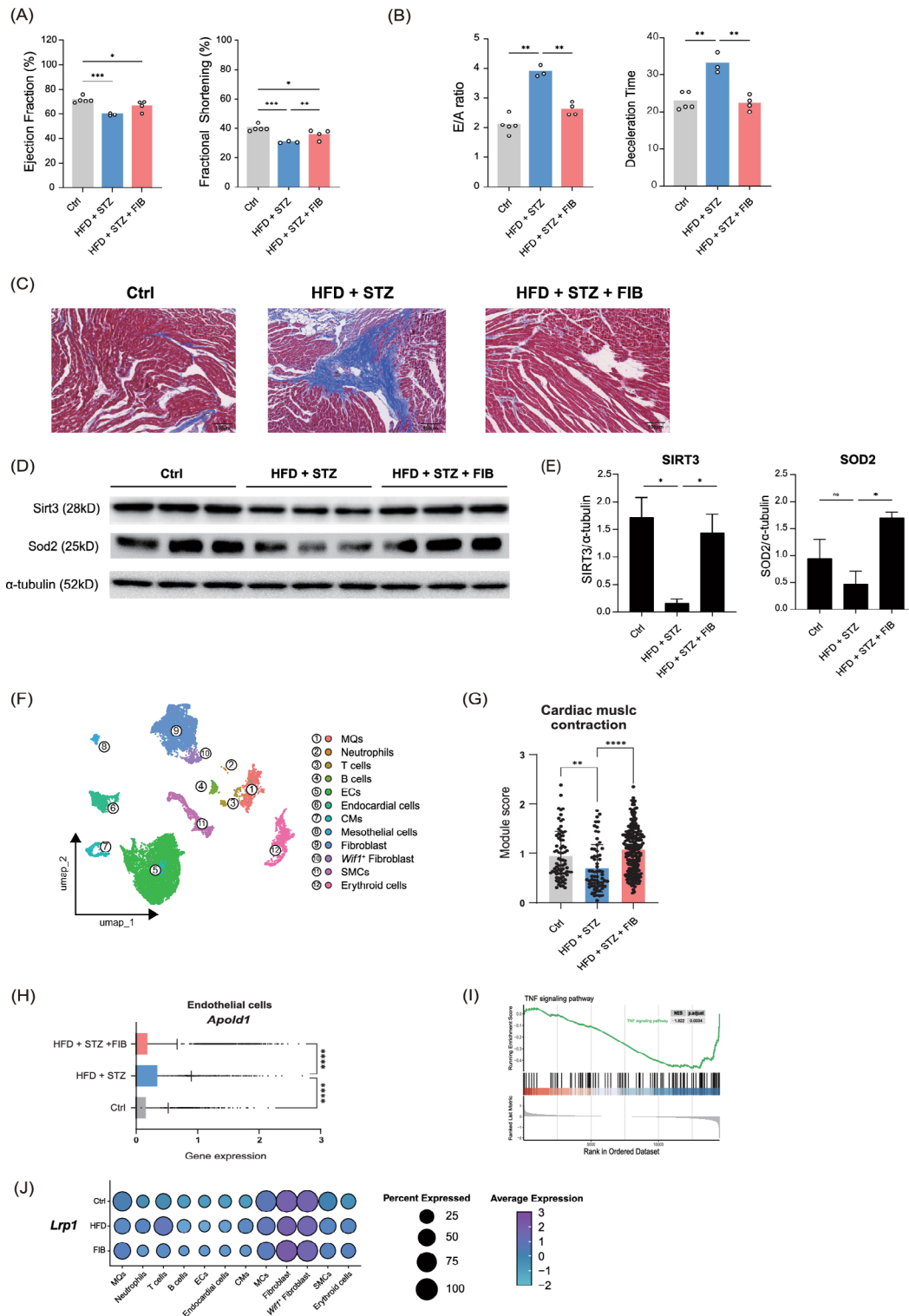


Fig. 5 Mouse **A** systolic and **B** diastolic function assessed by echocardiography. Mice were anesthetized and cardiac function was assessed using echocardiography (n=5 for control, n=3 for HFD + STZ, n=4 for FIB). **C** Masson's trichrome staining of mice heart, scale bar: 100 μ m. **D**, **E** Representative western blotting (top to bottom): Sirt3, SOD2, and loading control α -tubulin (n=3 per group). **F** UMAP plot for the integrated data of single cell RNA sequencing analysis (n=2 per group). **G** Bar plot showing module score related to cardiac muscle contraction. **H** The *Apold1* gene expression in endothelial cells in heart. **I** GSEA plot of TNF signaling pathway. **J** Dot plot of *Lrp1* gene expression in cardiac cells in heart. Ctrl Control; HFD high fat diet; STZ streptozotocin; FIB fenofibrate; MQ macrophage; EC endothelial cell; CM cardiomyocyte; MC Mesothelial cell; SMC smooth muscle cells. Data are presented as mean \pm SEM. ****P < 0.0001, ***P < 0.001, **P < 0.01, *P < 0.05 compared with Control. Significant differences were determined by using a two-way ANOVA

fibroblasts in diabetic heart. Fenofibrate treatment suppressed *Aplod1* expression and TNF signaling in EC cells. It also upregulates *Lrp1* expression in cardiac fibroblast.

Our nationwide population-based cohort study showed a significant association between fenofibrate treatment and a reduced risk of HF hospitalization compared with non-fenofibrate users in the general population who were also taking a statin. Furthermore, our subgroup analysis showed that the reduction in the risk of HF hospitalization was also significant in the obese population. These findings are consistent with previous clinical studies that have also reported the beneficial effects of fenofibrate in reducing the incidence of cardiovascular disease (CVD) in obese individuals (HR 0.83, 95% CI 0.78–0.88) [14]. Taken together, our results provide further evidence of the potential benefits of fenofibrate treatment in reducing the risk of HF hospitalization, particularly in the context of obesity.

About diabetes, recent two studies from the ACCORD-lipid trial reported beneficial effects of fenofibrate on the CVD outcomes in diabetes patients with statin [13, 50]. Marshall et al. reported that fenofibrate reduced the risk of major cardiovascular events such as nonfatal myocardial infarction, nonfatal stroke, or death from cardiovascular causes among patients with dyslipidemia (HR, 0.73; 95% CI, 0.56–0.95) [50]. Ferreira et al. reported that fenofibrate reduced the risk of composite outcome of HF hospitalization or cardiovascular death (HR, 0.64; 95% CI, 0.48–0.85) among diabetes patients receiving standard glucose-lowering strategy, but this was not significant among patients receiving intensive glucose-lowering strategy [13].

Our research has several limitations. Although our study provides valuable insights into the potential mechanisms underlying PPAR α action on obese and diabetic mouse hearts through cardiac tissue transcriptome analysis, some points require further investigation. We have identified possible candidate genes, including *Nr4a* and *Tnfa*, which show statistical significance in our analyses. However, additional *in vitro* and *in vivo* experiments are needed to further validate these predicted mechanisms and to fully elucidate the pathways through which fenofibrate exerts its beneficial effects. Although fenofibrate directly protected cardiomyocytes against glucolipototoxicity in our *in vitro* assays, we did not analyze the secondary effects of fenofibrate on other peripheral tissues, including pancreatic beta cells and liver, in our mouse study. Further studies are needed to evaluate the direct role of fenofibrate on the heart using heart-specific PPAR α knockout mice. Our single-cell RNA sequencing showed a low population of cardiomyocytes. This may be due to tissue damage during tissue dissociation processes, which may also affect the status of other cardiac cells. Therefore, other RNA sequencing methods, such as

single-nucleus RNA sequencing, are needed to validate our findings and provide a more accurate representation of cardiac cell populations. In addition, our clinical data were limited to baseline biological parameters, and we lacked follow-up information on blood glucose and lipid levels. This precluded the inclusion of drug response to fenofibrate, such as changes in plasma TG levels, in our study cohort. Therefore, further prospective cohort studies are warranted to evaluate the effect of fenofibrate based on drug response.

Conclusions

In conclusion, our results demonstrate that fenofibrate, a PPAR α agonist, significantly protects the structural and functional integrity of the heart against glucolipototoxicity in cardiometabolic dysfunction of mice. Fenofibrate effectively attenuates cardiac steatosis, oxidative stress and consequent cellular apoptosis associated with obesity and diabetes. Upstream regulator analyses revealed that TNF is a significant predicted inhibitor. Single-cell RNA sequencing analysis revealed that PPAR α activation upregulates *Lrp1* expression in cardiac fibroblasts. These findings suggest novel therapeutic candidates for the treatment of cardiometabolic dysfunction. Notably, clinical evidence suggests that the beneficial effects of fenofibrate on the prognosis of CVD, such as HF hospitalization, are significant. Taken together, these results highlight the potential of targeting PPAR α pathways as a promising strategy for the prevention of HF development and progression.

Abbreviations

HF	Heart failure
PPAR α	Peroxisome proliferator-activated receptor alpha
ECHOES	UK community-based Electrocardiographic Heart of England study
GIST	Gwangju Institute of Science and Technology
GTT	Glucose tolerance test
DCFDA	2',7'-Dichlorofluorescein diacetate
ROS	Reactive oxidative species
AST	Aspartate aminotransferase
ALT	Alanine aminotransferase
T-BIL	Total bilirubin
DEGs	Differentially expressed genes
GSEA	Gene Set Enrichment Analysis
GO	Gene Ontology
KEGG	Kyoto Encyclopaedia of Genes and Genomes
URA	Upstream regulatory analysis
NHID	National Health Insurance Database
TG	Triglyceride
Foxo3a	Forkhead Box O3
Zfp69	Zinc finger protein 69
Gck	Glucokinase
Cth	Cystathionine-gamma-ligase
Fos	Fos proto-oncogene
Nr4a1	Nuclear receptor subfamily 4 group A member 1
Aplod1	Apolipoprotein L domain containing 1
Ptger2	Prostaglandin E receptor 2
Gfi1	Growth factor-independent 1 transcriptional repressor
TNF	Tumor necrosis factor
Ifnb1	Interferon beta 1
Lrp1	Low-density lipoprotein receptor-related protein 1

Supplementary Information

The online version contains supplementary material available at <https://doi.org/10.1186/s12933-024-02417-6>.

Additional file 1

Author contributions

K.H., S.W.C., and C.-M.O. contributed to the conceptual design of the project and the experiments described in the manuscript. The experiments were performed by J.P., W.J. and H. S.. The data were analyzed by J.P., S.M., H.S. Y.K., and S.C.. The manuscript was written by S.M., and C.-M.O.. Then, the manuscript was edited and critically evaluated by K.H., H.K., S.W.C., and C.-M.O.. All authors read and approved the final version of the manuscript.

Funding

This research was supported by the Basic Science Research Program through the National Research Foundation of Korea (NRF), funded by the Ministry of Education (2020R1C1C1004999, 2020R1C1C1015104), by KHIDI-AZ Diabetes Research Program, by Young Medical Scientist Research Grant through the Daewoong Foundation (DFY2107P), by NRF grant funded by the Korea government (Ministry of Science and ICT) (2020R1F1A1071659) and by a National Research Council of Science & Technology (NST) grant by the Korean government (MSIT) (No. CAP23021-000).

Data availability

The sequencing data is accessible via the Gene Expression Omnibus database (GSE220127).

Declarations

Conflict of interests

The authors declare no competing interests.

Received: 13 May 2024 / Accepted: 22 August 2024

Published online: 16 September 2024

References

1. Malik A, Brito D, Vaqar S, Chhabra L. Congestive heart failure. 2017.
2. Jones NR, Hobbs FR, Taylor CJ. Prognosis following a diagnosis of heart failure and the role of primary care: a review of the literature. *BJGP Open*. 2017. <https://doi.org/10.3399/bjgpopen17X101013>.
3. Taylor CJ, Roalfe AK, Iles R, Hobbs FR. Ten-year prognosis of heart failure in the community: follow-up data from the Echocardiographic Heart of England Screening (ECHOES) study. *Eur J Heart Fail*. 2012;14(2):176–84.
4. Shah KS, Xu H, Matsouaka RA, Bhatt DL, Heidenreich PA, Hernandez AF, Devore AD, Yancy CW, Fonarow GC. Heart failure with preserved, borderline, and reduced ejection fraction: 5-year outcomes. *J Am Coll Cardiol*. 2017;70(20):2476–86.
5. Lavie CJ, Milani RV, Ventura HO. Obesity and cardiovascular disease: risk factor, paradox, and impact of weight loss. *J Am Coll Cardiol*. 2009;53(21):1925–32.
6. Kenny HC, Abel ED. Heart failure in type 2 diabetes mellitus: impact of glucose-lowering agents, heart failure therapies, and novel therapeutic strategies. *Circ Res*. 2019;124(1):121–41.
7. Larsen TS, Jansen KM. Impact of obesity-related inflammation on cardiac metabolism and function. *J Lipid Atheroscler*. 2021;10(1):8.
8. Finck BN. The PPAR regulatory system in cardiac physiology and disease. *Cardiovasc Res*. 2007;73(2):269–77.
9. Sarma S, Ardehali H, Gheorghiane M. Enhancing the metabolic substrate: PPAR- α agonists in heart failure. *Heart Fail Rev*. 2012;17:35–43.
10. Han L, Shen W-J, Bittner S, Kraemer FB, Azhar S. PPARs: regulators of metabolism and as therapeutic targets in cardiovascular disease. Part I: PPAR- α . *Future Cardiol*. 2017;13(3):259–78.
11. Parry TL, Desai G, Schisler JC, Li L, Quintana MT, Stanley N, Lockyer P, Patterson C, Willis MS. Fenofibrate unexpectedly induces cardiac hypertrophy in mice lacking MuRF1. *Cardiovasc Pathol*. 2016;25(2):127–40.
12. Huang W-P, Yin W-H, Chen J-S, Huang P-H, Chen J-W, Lin S-J. Fenofibrate attenuates doxorubicin-induced cardiac dysfunction in mice via activating the eNOS/EPC pathway. *Sci Rep*. 2021;11(1):1159.
13. Ferreira JP, Vasques-Nóvoa F, Ferrão D, Saraiva F, Falcão-Pires I, Neves JS, Sharma A, Rossignol P, Zannad F, Leite-Moreira A. Fenofibrate and heart failure outcomes in patients with type 2 diabetes: analysis from ACCORD. *Diabetes Care*. 2022;45(7):1584–91.
14. Kim K-S, Hong S, Han K, Park C-Y. Fenofibrate add-on to statin treatment is associated with low all-cause death and cardiovascular disease in the general population with high triglyceride levels. *Metabolism*. 2022;137: 155327.
15. Bogdanov P, Hernández C, Corraliza L, Carvalho AR, Simó R. Effect of fenofibrate on retinal neurodegeneration in an experimental model of type 2 diabetes. *Acta Diabetol*. 2015;52:113–22.
16. Lamberti M, Porto S, Marra M, Zappavigna S, Grimaldi A, Feola D, Pesce D, Naviglio S, Spina A, Sannolo N. 5-Fluorouracil induces apoptosis in rat cardiocytes through intracellular oxidative stress. *J Exp Clin Cancer Res*. 2012;31:1–8.
17. Gao S, Ho D, Vatner DE, Vatner SF. Echocardiography in mice. *Curr Protoc Mouse Biol*. 2011;1(1):71–83.
18. Stouffer SA, Suchman EA, DeVinney LC, Star SA, Williams Jr RM. The American soldier: Adjustment during army life. (studies in social psychology in world war ii), vol. 1. 1949.
19. Huang DW, Sherman BT, Lempicki RA. Systematic and integrative analysis of large gene lists using DAVID bioinformatics resources. *Nat Protoc*. 2009;4(1):44–57.
20. Krämer A, Green J, Pollard J Jr, Tugendreich S. Causal analysis approaches in ingenuity pathway analysis. *Bioinformatics*. 2014;30(4):523–30.
21. Kim MK, Han K, Lee S-H. Current trends of big data research using the Korean National Health Information Database. *Diabetes Metab J*. 2022;46(4):552–63.
22. Wei C-D, Li Y, Zheng H-Y, Tong Y-Q, Dai W. Palmitate induces H9c2 cell apoptosis by increasing reactive oxygen species generation and activation of the ERK1/2 signaling pathway. *Mol Med Rep*. 2013;7(3):855–61.
23. Li R-j, Yang J, Yang Y, Ma N, Jiang B, Sun Q-w, Li Y-j. Speckle tracking echocardiography in the diagnosis of early left ventricular systolic dysfunction in type II diabetic mice. *BMC Cardiovasc Disord*. 2014;14:1–8.
24. Keating GM. Fenofibrate: a review of its lipid-modifying effects in dyslipidemia and its vascular effects in type 2 diabetes mellitus. *Am J Cardiovasc Drugs*. 2011;11:227–47.
25. Krafczyk N, Klotz LO. FOXO transcription factors in antioxidant defense. *IUBMB Life*. 2022;74(1):53–61.
26. Tate M, Prakoso D, Willis AM, Peng C, Deo M, Qin CX, Walsh JL, Nash DM, Cohen CD, Rofo AK, et al. Characterising an alternative murine model of diabetic cardiomyopathy. *Front Physiol*. 2019;10:1395.
27. Wei K-H, Lin I-T, Chowdhury K, Lim KL, Liu K-T, Ko T-M, Chang Y-M, Yang K-C, Lai S-LB. Comparative single-cell profiling reveals distinct cardiac resident macrophages essential for zebrafish heart regeneration. *Elife*. 2023;12: e84679.
28. Wang M, Li Y, Li S, Lv J. Endothelial dysfunction and diabetic cardiomyopathy. *Front Endocrinol*. 2022;13: 851941.
29. Knapp M, Tu X, Wu R. Vascular endothelial dysfunction, a major mediator in diabetic cardiomyopathy. *Acta Pharmacol Sin*. 2019;40(1):1–8.
30. Duchateau PN, Pullinger CR, Orellana RE, Kunitake ST, Naya-Vigne J, O'Connor PM, Malloy MJ, Kane JP. Apolipoprotein L, a new human high density lipoprotein apolipoprotein expressed by the pancreas: identification, cloning, characterization, and plasma distribution of apolipoprotein L. *J Biol Chem*. 1997;272(41):25576–82.
31. Fan Z, Ardicoglu R, Batavia AA, Rust R, von Ziegler L, Waag R, Zhang J, Desgeorges T, Sturman O, Dang H. The vascular gene *Apold1* is dispensable for normal development but controls angiogenesis under pathological conditions. *Angiogenesis*. 2023;26(3):385–407.
32. Li C, Su F, Zhang L, Liu F, Fan W, Li Z, Ma J. Identifying potential diagnostic genes for diabetic nephropathy based on hypoxia and immune status. *J Inflamm Res*. 2021;14:6871–91.
33. von Ziegler LM, Floriou-Servou A, Waag R, Das Gupta RR, Sturman O, Gapp K, Maat CA, Kockmann T, Lin H-Y, Duss SN. Multiomic profiling of the acute stress response in the mouse hippocampus. *Nat Commun*. 2022;13(1):1824.
34. Au DT, Ying Z, Hernández-Ochoa EO, Fondrie WE, Hampton B, Migliorini M, Galisteo R, Schneider MF, Daugherty A, Rateri DL. LRP1 (low-density lipoprotein receptor-related protein 1) regulates smooth muscle contractility by modulating Ca²⁺ signaling and expression of cytoskeleton-related proteins. *Arterioscler Thromb Vasc Biol*. 2018;38(11):2651–64.
35. Wujak L, Schnieder J, Schaefer L, Wygrecka M. LRP1: A chameleon receptor of lung inflammation and repair. *Matrix Biol*. 2018;68:366–81.

36. McGavock JM, Lingvay I, Zib I, Tillery T, Salas N, Unger R, Levine BD, Raskin P, Victor RG, Szczepaniak LS. Cardiac steatosis in diabetes mellitus: a 1H-magnetic resonance spectroscopy study. *Circulation*. 2007;116(10):1170–5.
37. Li C, Liu H, Xu F, Chen Y. The role of lipotoxicity in cardiovascular disease. *Emerg Crit Care Med*. 2022;2(4):214–8.
38. Arner P, Rydén M. Fatty acids, obesity and insulin resistance. *Obes Facts*. 2015;8(2):147–55.
39. Zhang D, Niu S, Ma Y, Chen H, Wen Y, Li M, Zhou B, Deng Y, Shi C, Pu G. Fenofibrate improves insulin resistance and hepatic steatosis and regulates the Let-7/SERCA2b axis in high-fat diet-induced non-alcoholic fatty liver disease mice. *Front Pharmacol*. 2022;12: 770652.
40. Park C, Zhang Y, Zhang X, Wu J, Chen L, Cha D, Su D, Hwang M-T, Fan X, Davis L. PPAR α agonist fenofibrate improves diabetic nephropathy in db/db mice. *Kidney Int*. 2006;69(9):1511–7.
41. Zheng S, Ren X, Han T, Chen Y, Qiu H, Liu W, Hu Y. Fenofibrate attenuates fatty acid-induced islet β -cell dysfunction and apoptosis via inhibiting the NF- κ B/MIF dependent inflammatory pathway. *Metabolism*. 2017;77:23–38.
42. Jeong S, Yoon M. Fenofibrate inhibits adipocyte hypertrophy and insulin resistance by activating adipose PPAR α in high fat diet-induced obese mice. *Exp Mol Med*. 2009;41(6):397–405.
43. Zong X, Cheng K, Yin G, Wu Z, Su Q, Yu D, Liao P, Hu W, Chen Y. SIRT3 is a downstream target of PPAR- α implicated in high glucose-induced cardiomyocyte injury in AC16 cells. *Exp Ther Med*. 2020;20(2):1261–8.
44. Sun W, Liu C, Chen Q, Liu N, Yan Y, Liu B. SIRT3: a new regulator of cardiovascular diseases. *Oxid Med Cell Longev*. 2018;2018(1):7293861.
45. Zhang C, Zhang B, Zhang X, Sun G, Sun X. Targeting orphan nuclear receptors NR4As for energy homeostasis and diabetes. *Front Pharmacol*. 2020;11: 587457.
46. Men L, Hui W, Guan X, Song T, Wang X, Zhang S, Chen XJG. Cardiac transcriptome analysis reveals Nr4a1 mediated glucose metabolism dysregulation in response to high-fat diet. *Genes*. 2020;11(7):720.
47. Medzikovic L, de Vries CJ, de Waard V. NR4A nuclear receptors in cardiac remodeling and neurohormonal regulation. *Trends Cardiovasc Med*. 2019;29(8):429–37.
48. Grabacka M, Pierzchalska M, Plonka PM, Pierzchalski P. The role of PPAR alpha in the modulation of innate immunity. *Int J Mol Sci*. 2021;22(19):10545.
49. Zambon A, Gervois P, Pauletto P, Fruchart J-C, Staels B. Modulation of hepatic inflammatory risk markers of cardiovascular diseases by PPAR- α activators: clinical and experimental evidence. *Arterioscler Thromb Vasc Biol*. 2006;26(5):977–86.
50. Elam MB, Ginsberg HN, Lovato LC, Corson M, Largay J, Leiter LA, Lopez C, O'Connor PJ, Sweeney ME, Weiss D. Association of fenofibrate therapy with long-term cardiovascular risk in statin-treated patients with type 2 diabetes. *JAMA Cardiol*. 2017;2(4):370–80.

Publisher's Note

Springer Nature remains neutral with regard to jurisdictional claims in published maps and institutional affiliations.